Structure and Properties of Poly(*o*-methoxyaniline)–Clay Nanocomposite Materials

Jui-Ming Yeh, Chih-Ping Chin

Department of Chemistry and Center for Nanotechnology at CYCU, Chung-Yuan Christian University, Chung Li, 320, Taiwan, Republic of China

Received 4 February 2002; accepted 28 May 2002

ABSTRACT: In this study, we prepared a series of polymer–clay nanocomposite (PCN) materials that consisted of an emeraldine base of poly(*o*-methoxyaniline) and layered montmorillonite. Organic *o*-methoxyaniline monomers were first intercalated into the interlayer regions of organophilic clay hosts followed by a one-step *in situ* oxidative polymerization. The as-synthesized PCN materials were subsequently characterized by FTIR spectroscopy, wide-angle powder X-ray diffraction, and transmission electron microscopy. The molecular weights of PMA extracted from PCN materials and bulk PMA were determined by GPC with THF as eluant. Effects of the material composition on the thermal stability, flame resistance, electrical conductivity, and corrosion inhibition performance of PMA, along with a series of PCN materials in the form of fine powder and coating, were also studied by TGA, limiting oxygen index measurements, four-point probe technique, and electrochemical corrosion measurements, respectively. Morphological images of as-synthesized materials were also investigated by SEM. © 2003 Wiley Periodicals, Inc. J Appl Polym Sci 88: 1072–1080, 2003

Key words: nanocomposite; clay; conducting polymer; corrosion inhibition; flame resistance

INTRODUCTION

The manufacture of new materials with enhanced properties and performance is a continually expanding area at the interface of chemistry and materials science. A significant advance in this field has been the synthesis of nanocomposites. Recently, polymer–clay hybrid nanocomposite (PCN) materials have evoked extensive research interests because of their unique characteristics in the creation of potentially commercial applications. PCN materials have been reported to boost the thermal stability,[1] mechanical strength,[2] molecular barrier,[3] flame resistance,[4] and corrosion inhibition[5] properties of polymers by incorporating small amounts of clay platelets in the polymer matrix. The historical development of PCN materials can be traced back to 1990 based on the studies of polyamide–clay nanocomposite materials reported by Toyota's research group.[6]

On the other hand, electrically conducting polymers have been the focus of extensive studies since the discovery that the conductivity of polyacetylene achieves the metallic region upon doping by oxidizing or reducing agents. Some specific conducting polymers (e.g., polyanilines, polythiophene, and polypyrrole) have been found to display interesting photoelectric properties. Wei et al.[7] demonstrated the corrosion-inhibition effect of polyaniline by carrying out a series of electrochemical measurements on the polyaniline-coated cold-rolled steel (CRS) coupons under various corrosion conditions. However, polyaniline has always been regarded as an intractable material because of its poor solubility in common organic solvents. Many soluble derivatives of polyaniline are therefore synthesized by polymerizing ring- or nitrogen-substituted aniline monomers and/or by copolymerization.[8,9] Accordingly, one ring-substituted polyaniline derivative, poly(*o*-methoxyaniline) (PMA), has attracted considerable attention lately because of its good solubility in common organic solvents. The corrosion inhibition of iron in acidic media using PMA was also reported by Sathiyanarayanan et al.[10]

Recently, polymer–clay nanocomposites that consisted of different layered materials and conducting polymers (e.g., polyaniline,[5,11–17] polythiophene, polypyrrole[18]) were found to exhibit novel properties, which can be obtained from the interaction of the two dissimilar chemical components at the molecular level. In this study, we prepared a series of poly(*o*-methoxyaniline)–clay nanocomposite (PCN) materials by effectively dispersing the inorganic nanolayers of montmorillonite (MMT) clay in organic PMA matrix by *in situ* oxidative polymerization. The as-synthesized PCN materials were characterized by FTIR spectroscopy, wide-angle X-ray diffraction (XRD), and transmission electron microscopy (TEM). The molec-

Correspondence to: J.-M. Yeh (juiming@cycu.edu.tw).
Contract grant sponsor: NSC; contract grant number: 89-2113-M-033-014.

Journal of Applied Polymer Science, Vol. 88, 1072–1080 (2003)

ular weights of PMA extracted from PCN materials and bulk PMA were determined by gel permeation chromatography (GPC) with THF as eluant. Effects of the material composition on the thermal stability, flame resistance, electrical conductivity, and corrosion-inhibition performance of PMA along with a series of PCN materials, in the form of fine powder and coating, were studied by thermogravimetric analysis (TGA), limiting oxygen index (LOI) measurements, four-point probe technique, and electrochemical corrosion measurements, respectively. Morphological images of as-synthesized materials were also investigated by scanning electron microscopy (SEM).

EXPERIMENTAL

Chemicals and instrumentations

Terahydrofuran (THF), 1-methyl-2-pyrrolidinone (NMP, 99.97%; Tedia), lithium chloride (99%; Acros), methanol (ACS grade; Tedia), and ammonium peroxodisulfate (Showa) were used as received without further purification. *O*-Methoxyaniline (99%; Acros) was doubly distilled under reduced pressure. Ammoniaque solution (25%; Riedel-de Haën, Seelze, Germany) and hydrochloric acid (37%; Riedel-de Haën) were applied to prepare the 1.0*M* NH_4OH and 1.0*M* HCl aqueous solution. The MMT clay PK805, which consisted of a CEC value of 98 meq/100 g and a unit cell formula $[Na_{0.48}K_{0.01}Ca_{0.01}{\cdot}Ti_{0.01}]$ $(Fe_{0.20}Al_{1.44}Mg_{0.31})$ $(Si_{3.93}Al_{0.07})$ O_{10} $(OH)_2{\cdot}ZH_2O$, was supplied by Paikong Ceramic Company (Taiwan). The intercalating agent, the chemical structure of which is $C_{11}H_{23}CONH(CH_2)_2N^+(CH_3)_2CH_2CHOHCH_2SO_3^-$ (cocamidopropyl-hydroxysultaine), was supplied by Industrial Technology Research Institute (ITRI, Taiwan). The wide-angle powder XRD study of the samples was carried out by a Rigaku D/MAX-3C OD-2988N X-ray diffractometer (Rigaku, Japan) with copper target and Ni filter at a scanning rate of 4°/min. The samples for TEM study were first prepared by putting poly(*o*-methoxyaniline)–clay powder into poly(methyl methacrylate) (PMMA) capsules and by curing the PMMA at 100°C for 24 h in a vacuum oven. The cured PMMA samples containing PCN materials were then microtomed with Reichert-jumg Ultracut-E into slices (60–90 nm thick). Subsequently, one layer of carbon about 10 nm thick was deposited onto these slices on mesh 100 copper nets for TEM observations on a JEOL-200FX (JEOL, Peabody, MA) with an acceleration voltage of 120 kV. A Seiko thermal analysis system (Seiko Instruments, Japan), equipped with model TG/DTA 220 thermogravimetric analyzer, was employed to perform the thermal analyses under air flow. The programmed heating rate was 20°C/min in most cases.

The standard electrochemical corrosion measurements of PCN-coated CRS coupons were carried out by a Radiometer VoltaLab 21 potentiostat/galvanostat in a standard corrosion cell equipped with two graphite rod counter electrodes and a saturated calomel electrode (SCE) as well as the working electrode. The molecular weights of polymer extracted from all samples as well as bulk poly(*o*-methoxyaniline) were determined by GPC. A Waters gel permeation chromatograph model 2 II (Waters Chromatography Division/Millipore, Medford, MA), equipped with a model 590 programmable solvent delivery module, a differential refractometer detector, and an Ultrastyragel linear packed column, was employed to performed the GPC studies. Temperatures of the GPC column and detector were kept at 35°C. The molecular weight of the polymer was calculated based on the calibration with monodisperse polystyrene standards. Molecular weights of the standard polystyrene samples were 5000, 8000, 70,000, and 200,000. FTIR spectra were recorded from pressed KBr pellets using a Bio-Rad FTS-7 FTIR spectrometer (Bio-Rad, Hercules, CA). Conductivity measurements were made on a four-point probe connected to a Keithley 2400 voltmeter constant-current source system (Keithley Metrabyte, Taunton, MA). The sample in the form of compacted disk pellets was 12.6 mm in diameter and about 1 mm thick. Three measurements were made on each of duplicate samples. LOI values were measured on a United States Testing 8100 flame meter by a modified method that was previously investigated in the literature.[19,20] The percentage in the O_2/N_2 mixture deemed sufficient to sustain the flame was taken as the LOI. Microstructure of the materials was imaged through a JEOL SEM JSM-6330F, operated with a high-tension voltage of 10 kV.

Preparation of poly(*o*-methoxyaniline)

In a typical procedure, 10 mL of doubly distilled *o*-methoxyaniline (0.100 mol) was dissolved in 600 mL of 1.0*M* HCl and the mixture was precooled to about 0°C in an ice bath. A solution (200 mL) of 5.6 g (0.025 mol) $(NH_4)_2S_2O_8$ in 1.0*M* HCl was added to the aniline solution dropwise over a period of 15 min with vigorously magnetic stirring. After about 2 h, the precipitate was collected on a Buchner funnel. Upon drying under dynamic vacuum at room temperature, the HCl-doped PMA was obtained as a green powder. The HCl-doped PMA was subsequently converted into an emeraldine base form of PMA by stirring about 3 g of the emeraldine hydrochloride fine powder in an excess amount (500 mL) of 1.0*M* ammonium hydroxide at room temperature for 3 h. Upon filtering and drying under dynamic vacuum for 48 h, the emeraldine base of PMA was obtained as a blue powder.

Preparation of organophilic clay and PCN materials, and recovery of polymers

The typical procedure to synthesize organophilic clay and PCN materials, and the recovery of polymers followed our previously published results.[5(a),(c)]

Preparation of coatings and electrochemical measurements[5]

As a representative procedure to prepare sample-coated coupons for electrochemical measurements, the emeraldine base of PMA and PCN fine powders were dissolved in NMP to give typically 1 wt % solutions. The solutions were cast dropwise onto the CRS coupons (1 × 1 cm) followed by drying in air for 48 h, to give coatings of about 10 μm in thickness. Coated and uncoated coupons were then mounted to the working electrode so that only the coated side of the coupon was in direct contact with the electrolyte. The edges of the coupons were sealed with superfast epoxy cement (trade name SPAR). All electrochemical measurements were performed at room temperature. The electrolyte was NaCl (5 wt %) aqueous solution. The open circuit potential (OCP) at the equilibrium state of the system was recorded as the corrosion potential (E_{corr} in V versus SCE). Polarization resistance (R_p in Ω/cm^2) was measured by sweeping the applied potential from 20 MV below to 20 MV above the E_{corr} at a scan rate of 500 MV/min and recording the corresponding current change. The R_p value was obtained from the slope of the potential–current plot. The corrosion current (I_{corr}) was determined by superimposing a straight line along the linear portion of the cathodic or anodic curve and extrapolating it through E_{corr}. The corrosion rate [R_{corr}, in milli-inches per year (MPY)] was calculated from the following equation:

$$R_{corr}\ (\mathrm{MPY}) = [0.13 I_{corr}(\mathrm{E.W.})]/[Ad]$$

where E.W. is the equivalent weight (in g/eq), A is the area (in cm^2), and d is the density (in g/cm^3).

Morphological image studies of coatings

The emeraldine base of polyaniline and PCN fine powders were dissolved in NMP under magnetic stirring at room temperature for 4 h to give typically 1 wt % solutions. The solutions were cast dropwise onto a specific substrate. Samples for morphological imaging studies of SEM were obtained by evaporating the solvent at 90–100°C under the fume hood for 24 h.

RESULTS AND DISCUSSION

The base forms of poly(*o*-methoxyaniline) can be represented by the following general formula, where R = –OCH_3:

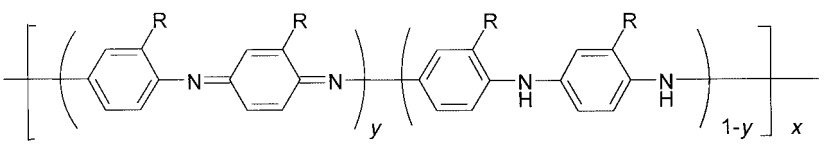

where the y value ranges from 1 for the fully oxidized polymer (so-called pernigraniline), to 0.5 for the half-oxidized polymer (emeraldine), and to 0 for the fully reduced polymer (leucoemeraldine). On the other hand, MMT is a clay mineral containing stacked silicate sheets measuring about 10 × 2180 Å (thickness × length)[21] and possessing both a high aspect ratio and a platey morphology. The chemical structure of MMT consists of two fused silica tetrahedral sheets sandwiching an edge-shared octahedral sheet of either magnesium or aluminum hydroxide. The Na^+ and Ca^{+2} residing in the interlayer regions can be replaced by organic cations such as alkylammonium or alkylphosphonium ions[5(b)] by a cationic-exchange reaction, to render the hydrophilic layered silicate organophilic. MMT has a high swelling capacity, which is important for efficient intercalation of the polymer, and is composed of stacked silicate sheets that provide improved thermal stability, mechanical strength, fire resistance, and molecular barrier properties.

To synthesize the PCN materials, organophilic clay was first prepared by a cationic-exchange reaction between the sodium cations of MMT clay and alkylammonium ions of the intercalating agent. Organic *o*-methoxyaniline monomers were subsequently intercalated into the interlayer regions of organophilic clay hosts and followed by a one-step oxidative polymerization. The composition of the PCN materials were varied from 0 to 10 wt % of clay with respect to the poly(*o*-methoxyaniline) content, as summarized in Table I.

Characterization

The representative FTIR spectra of the organophilic clay, bulk PMA, and PCN materials are given in Figure 1. The characteristic vibration bands of PMA are at 1118 cm^{-1} (C—O) and 1475 cm^{-1} (N—H), and those of MMT clay are shown at 1040 cm^{-1} (Si—O), 600 cm^{-1} (Al—O), and 420 cm^{-1} (Mg—O).[5] As the loading of MMT clay is increased, the stronger intensities of

TABLE I
Relations of the Composition of Poly(*o*-methoxyaniline)–MMT Clay Nanocomposite Materials with the E_{corr}, R_p, i_{corr}, and R_{corr} Measured by Electrochemical Methods

Compound code	Coating thickness[a] (μm)	Electrochemical corrosion measurements[b]			
		E_{corr} (mV)	R_p (kΩ/cm^2)	I_{corr} (μA/cm^2)	R_{corr} (MPY)
Bare	—	−641	0.80	44.40	86.140
PMA	12	−599	38.33	1.85	0.964
CLMA1	10	−544	53.91	1.20	0.043
CLMA3	9	−508	72.95	0.72	0.017
CLMA5	11	−500	85.87	0.46	0.011
CLMA10	10	−496	107.20	0.32	0.008

[a] As measured by a digimatic micrometer.
[b] Saturated calomel electrode was employed as reference electrode.

MMT clay vibration bands are found in the FTIR spectra of PCN materials. Figure 2 illustrates the wide-angle powder XRD patterns of organophilic clay and a series of PCN materials. In Figure 2, the powder XRD patterns do not show any diffraction peak at 2θ = 2–10°, as opposed to the diffraction PMA at 2θ = 5.90° (d spacing = 14.97 Å) for organophilic clay, indicating the possibility of having exfoliated silicate layers of organophilic clay dispersed in the PMA matrix. At 5 wt % organophilic clay, a small peak appeared at 2θ = 4.50°, corresponding to a d spacing of 19.62 Å. This implies that there was a small amount of organophilic clay that cannot be exfoliated in the PMA that exists in the form of an intercalated layer structure.

In Figure 3, transmission electron microscopy of PCN materials incorporating 5 wt % clay shows that the nanocomposite has a mixed nanomorphology. The observed domain of sample is found to exhibit the intercalated tactoids. In addition, some exfoliated morphology can also be observed.

MW determination of extracted and bulk polymers

Molecular weights of the various polymer samples recovered from the nanolayers of MMT clays were obtained by GPC analyses. The GPC elution patterns of the THF-soluble component displayed a single peak, corresponding to a molecular weight value. The molecular weights of extracted PMA were significantly lower than that of the bulk polymer, as shown in Figure 4, indicating the structurally restricted polymerization conditions in the intragallery region of the MMT clay[22] and/or the nature of clay–oligomer interactions, such as adsorption, during the polymerization reaction.

Thermal properties of fine powders (TGA, LOI)

Figure 5 shows a typical TGA thermogram of weight loss as a function of temperature for PCN materials along with PMA, as measured under an air atmo-

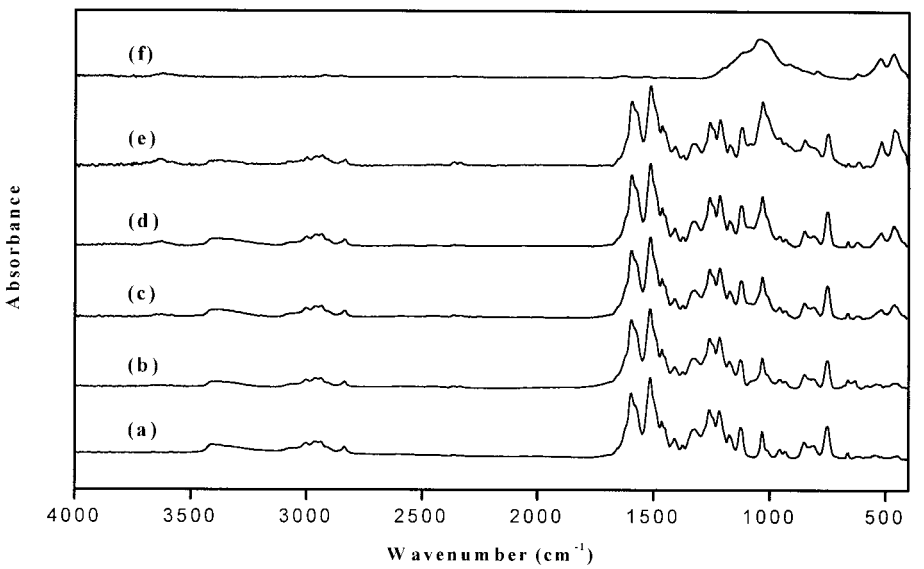

Figure 1 FTIR spectra of (a) PMA, (b) PMA1, (c) PMA3, (d) PMA5, (e) PMA10, and (f) organophilic clay.

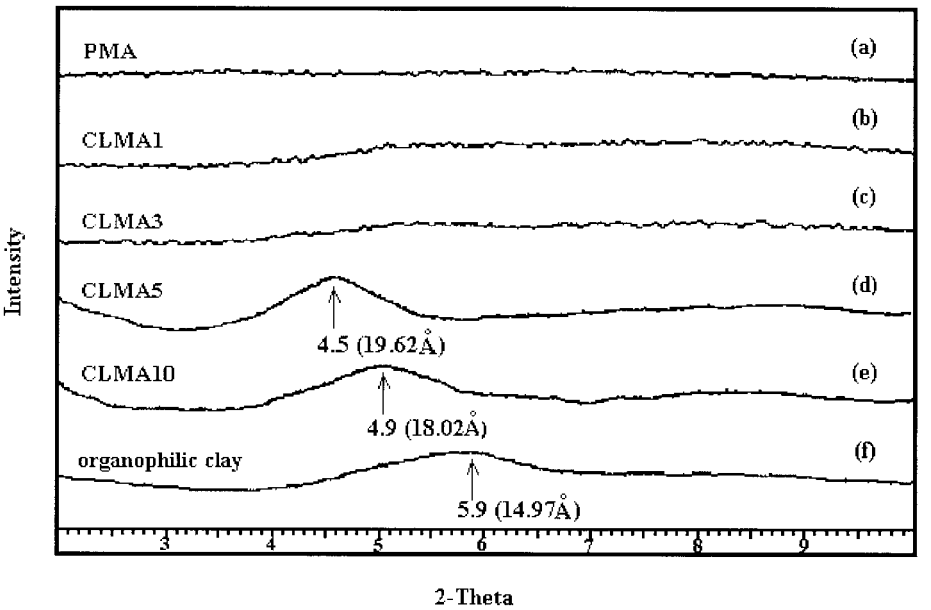

Figure 2 Wide-angle powder X-ray diffraction patterns ranging between $2\theta = 2°$ and $2\theta = 10°$ of organophilic, poly(*o*-methoxyaniline), and a series of poly(*o*-methoxyaniline)–clay nanocomposite materials.

sphere. In general, there were several stages of weight loss starting at about 250°C and ending at 900°C, which may correspond to the thermo-oxidative degradation of the intercalating agent at lower temperatures (e.g., around 200–300°C) followed by the structural decomposition of the polymer backbones at higher temperatures. Evidently, the onset of the thermal decomposition of those nanocomposites shifts slightly toward the lower temperature range than that of PMA, which confirms the significant lowering of polymeric molecular weight leading to a depression of thermal stability of intercalated polymer.[5] After about 700°C, the curves all became flat and mainly the inorganic residue (i.e., Al_2O_3, MgO, SiO_2, Fe_2O_3) remained. The flammability properties of the obtained PMA and PCN materials were examined by measuring the LOI value of the materials. A significant increase in LOI value was observed when the MMT clay platelets were effectively dispersed in the polymer matrix. This indicates that incorporation of MMT into the polymer matrix exhibits an efficient effect on leveling up the flame retardancy of the polymers. It is noteworthy that the LOI values increase with an increase in the MMT contents of the polymers, as shown in Figure 6. The common mechanism of flammability reduction was found by Gilman and Kashiwagi.[23] The nanocomposite structure tends to collapse during combustion. The multilayered carbonaceous–silicate structure was found to improve the performance of the char through structural reinforcement. This silicate-rich char may function as an excellent insulator and mass transport barrier, slowing the escape of the

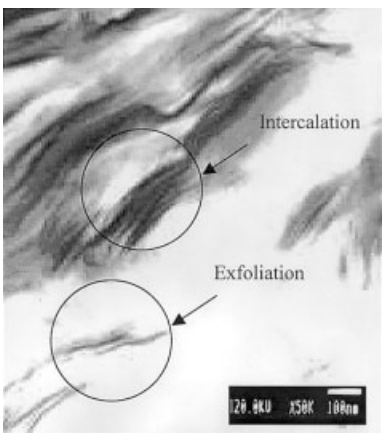

Figure 3 Transmission electron microscopy micrograph of PMA5.

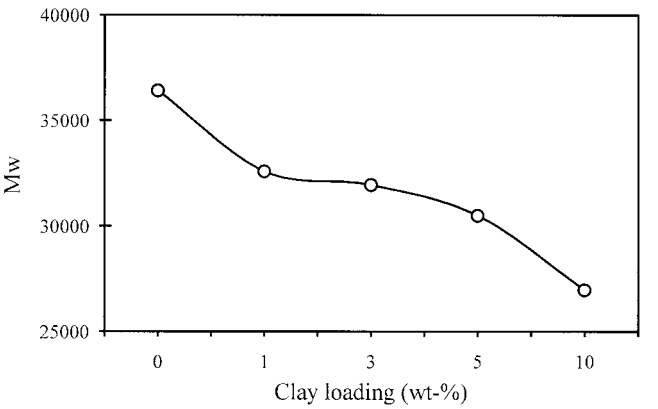

Figure 4 Weight-average molecular weight of extracted poly(*o*-methoxyaniline) and bulk polymer.

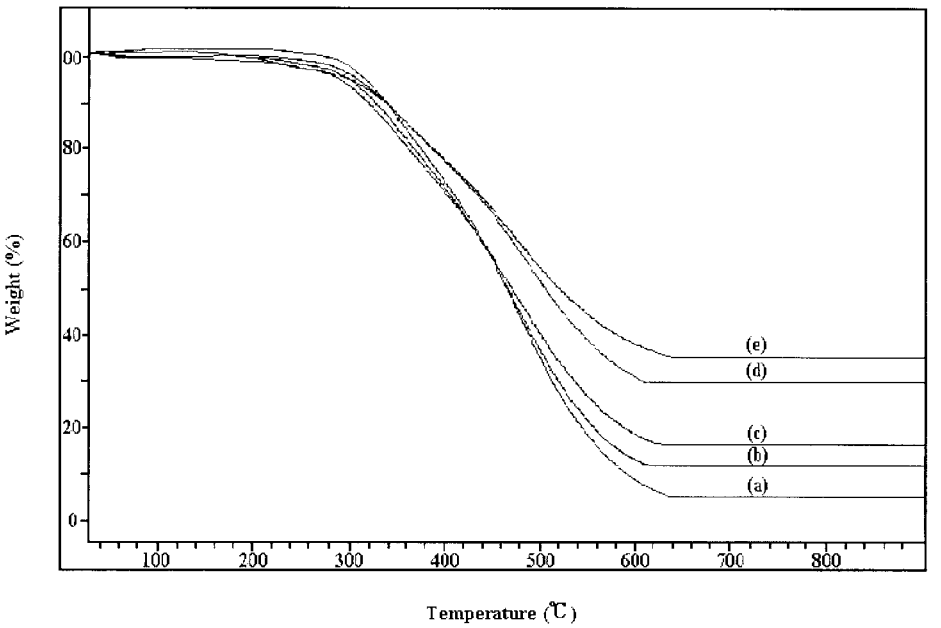

Figure 5 Relationship between the wt % and temperature as obtained from TGA measurements on the fine powders of (a) PMA, (b) PMA1, (c) PMA3, (d) PMA5, and (e) PMA10.

volatile products generated when the polymer decomposes.[24]

Electrical conductivity of doped powder-pressed pellets

We also found that the electrical conductivity of all the PCN materials is smaller than that of bulk polymer, as shown in Figure 7. This was expected because the MMT component is not electrically conductive and the incorporation of MMT clay platelets into the PMA matrix contributes to the decrease of polymer molecular weight, reflecting a decreased electrical conductivity.

Corrosion-inhibition properties of coatings

The corrosion-inhibition effect of sample-coated CRS coupons can be observed from the values of corrosion potential (E_{corr}), polarization resistance (R_p), corrosion current (I_{corr}), and corrosion rate (R_{corr}), as shown in Table I. The CRS coupon coated with an emeraldine base of PMA showed a higher E_{corr} value than that of the uncoated CRS. However, it exhibits a lower E_{corr} value than that of the specimen coated with PCN materials. For example, the PMA1-coated CRS displayed a high corrosion potential of about −544 MV at 30 min. Even after a 10-h measurement, the potential remained at about −550 MV. Such an E_{corr} value im-

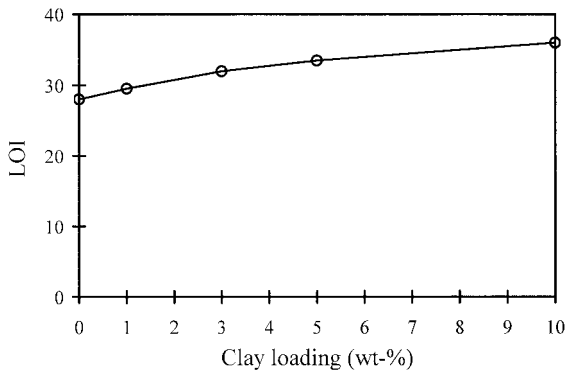

Figure 6 Relationship between the limiting oxygen index (LOI) value and clay loading as obtained from LOI measurements on the fine powders of (a) PMA, (b) PMA1, (c) PMA3, (d) PMA5, and (e) PMA10.

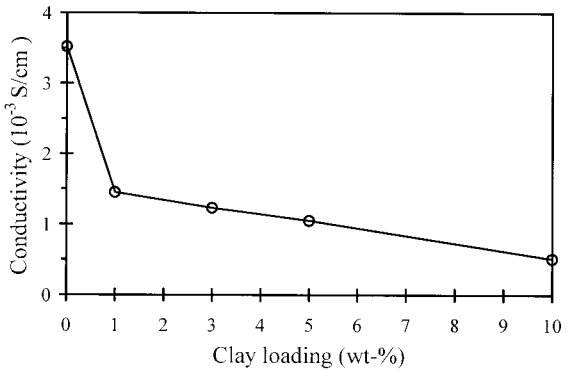

Figure 7 Relationship between the electrical conductivity and clay loading as obtained from four-point probe technique measurements on the HCl-doped powder-pressed pellets of (a) PMA, (b) PMA1, (c) PMA3, (d) PMA5, and (e) PMA10.

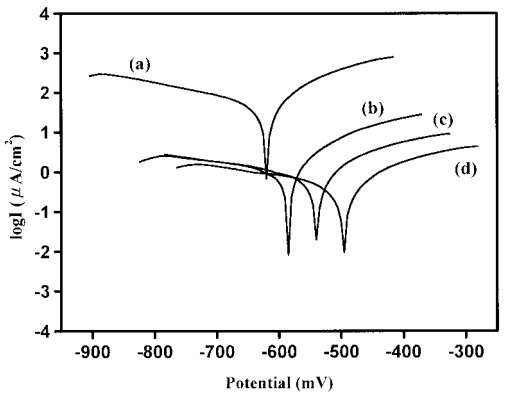

Figure 8 Tafel plots for (a) bare, (b) PMA-coated, (c) PMA1-coated, and (d) PMA3-coated CRS measured in 5 wt % NaCl aqueous solution.

plies that the PMA1-coated CRS is noble toward the electrochemical corrosion compared to the emeraldine base of PMA. The PMA1-coated CRS shows a polarization resistance (R_p) value of $5.4 \times 10^4\ \Omega/\text{cm}^2$ in 5 wt % NaCl, which is about 2 orders of magnitude greater than that of the uncoated CRS. The Tafel plots for (a) uncoated, (b) PMA-coated, (c) PMA1-coated, and (d) PMA3-coated CRS are shown in Figure 8. For example, the corrosion current (I_{corr}) of PMA1-coated CRS is about 1.2 $\mu\text{A}/\text{cm}^2$, which corresponds to a corrosion rate (R_{corr}) of about 0.043 MPY, as summarized in Table I. Electrochemical corrosion current values of PCN materials as coatings on CRS decreased gradually with further increases in clay loading. Visual observation of the corrosion products clearly displayed that the PCN samples exhibiting corrosion protection have a grayish oxide layer form over the bare exposed CRS surface, similar to what was observed by Wessling under the polyaniline dispersion coatings on steel.[25] The enhanced corrosion-inhibition effect of PCN materials compared to that of bulk PMA may be attributed to the dispersing silicate nanolayers of clay in the PMA matrix, which would increase the tortuosity of the diffusion pathway of O_2 molecules.[5]

Morphological image studies of coatings

The emeraldine base of poly(*o*-methoxyaniline) in the presence of MMT clay platelets exhibited higher crystallinity than that of bulk polymer, as illustrated in Figure 9 by powder XRD patterns ranging between $2\theta = 10°$ and $2\theta = 50°$. Furthermore, it should be noted that a further increase of dispersing MMT clay loading resulted in a further increase of polymer crystallinity. This obvious increase of polymer crystallinity may be associated with the strong heterogeneous nucleation effect[5] of the dispersing MMT platelets in the polymer matrix. The surface microstructures of polymer images can be examined by scanning electron microscopy, as shown in Figure 10. In Figure 10(a), the bulk polymer morphology at $\times$5000 magnification exhibits much larger crystals, relative to the small, fine crystals of PMA5, as shown in Figure 10(b). The reduction in crystal size of PMA5 may be attributed to the heterogeneous nucleation effect of the dispersing MMT platelets in the polymeric matrix.[26]

Conclusions

A series of nanocomposite materials, consisting of poly(*o*-methoxyaniline) (PMA) and layered montmo-

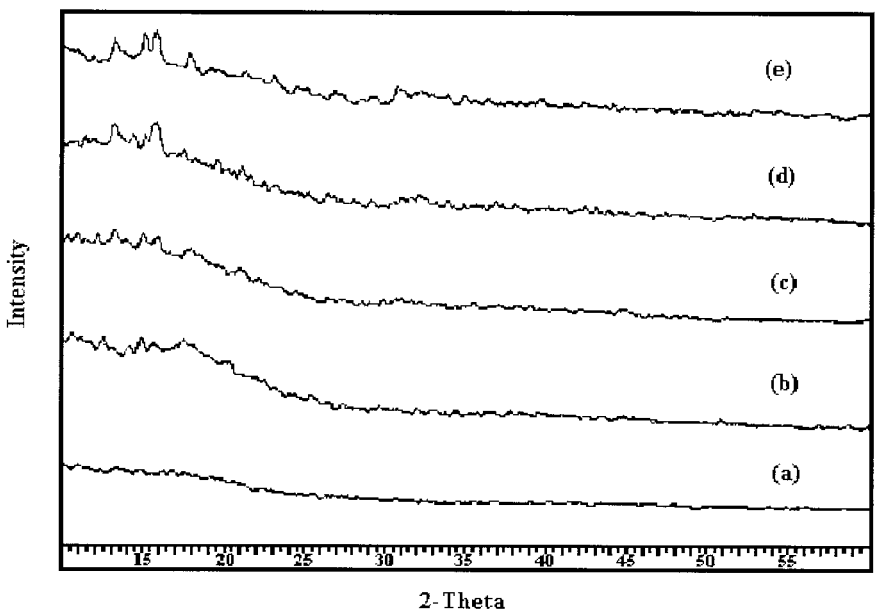

Figure 9 Wide-angle powder X-ray diffraction patterns ranging between $2\theta = 10°$ and $2\theta = 50°$ of organophilic, poly(*o*-methoxyaniline), and a series of poly(*o*-methoxyaniline)–clay nanocomposite materials.

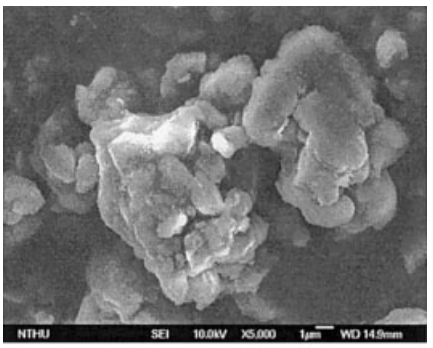

PMA/5000

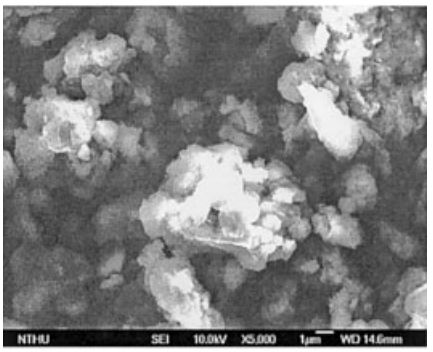

PMA5/5000

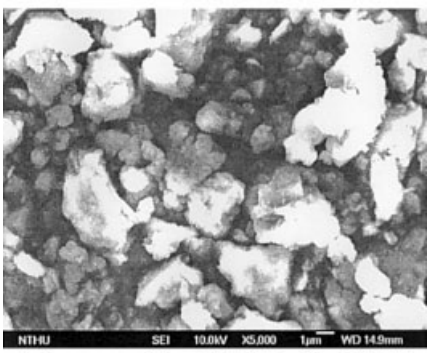

PMA10/5000

Figure 10 SEM micrographs (×5000 magnification) of (a) PMA, (b) PMA5, and (c) PMA10.

rillonite (MMT) clay, were prepared by effectively dispersing the inorganic nanolayers of MMT clay in organic PMA matrix by *in situ* oxidative polymerization. As-synthesized materials were characterized by infrared spectroscopy, wide-angle powder X-ray diffraction, and transmission electron microscopy. The molecular weights of extracted PMA exhibited a decreased molecular weight compared to that of the bulk PMA, indicating the structurally restricted polymerization conditions in the intragallery region of the MMT clay. The effect of material composition on the thermal stability, flame resistance, conductivity, and corrosion-inhibition effect of PMA along with a series of PCN materials in the form of coating and fine powder, were also studied by TGA, LOI, four-point probe technique, and electrochemical corrosion measurements, respectively. The thermal decomposition temperature (T_d) of those nanocomposites shifted slightly toward the lower temperature range than that of PMA based on the TGA studies, which confirmed the significant lowering of polymeric molecular weight leading to a depression of thermal stability of intercalated polymer. A significant increase in flame resistance was observed when the MMT clay platelets were effectively dispersed in the polymer matrix based on the studies of measurement of LOI value. We also found that the electrical conductivity of all the PCN materials is smaller than that of bulk polymer based on the four-point probe technique measurements. The coatings of PCN materials at low clay loading were found to offer good corrosion inhibition and show a better anticorrosion performance than that of the emeraldine base of bulk PMA. Morphological images of as-synthesized materials were investigated by scanning electron microscopy.

The financial support of this research by the NSC 89-2113-M-033-014 is gratefully acknowledged.

References

1. Tyan, H.-L.; Liu, Y.-C.; Wei, K.-H. Chem Mater 1999, 11, 1942.
2. (a) Wang, Z.; Pinnavaia, T. J Chem Mater 1998, 10, 3769; (b) Biswas, M.; Ray, S.-S. Adv Polym Sci 2001, 155, 167.
3. Lan, T.; Kaviratna, P. D.; Pinnavaia, T. J. Chem Mater 1994, 6, 573.
4. Gilman, J. W.; Jackson, C. L.; Morgan, A. B.; Hayyis, R., Jr.; Manias, E.; Giannelis, E. P.; Wuthenow, M.; Hilton, D.; Phillips, S. H. Chem Mater 2000, 12, 1866.
5. (a) Yeh, J.-M.; Liou, S.-J.; Lai, C.-Y.; Wu, P.-C.; Tsai, T. Y. Chem Mater 2001, 13, 1131; (b) Yeh, J.-M.; Liou, S.-J.; Lin, C.-Y.; Cheng, C.-Y.; Cheng, Y.-W.; Lee, K.-R. Chem Mater 2002, 14, 154; (c) Yeh, J.-M.; Chen, C.-L.; Chen, Y.-C.; Ma, C.-Y.; Lee, K.-R.; Wei, Y.; Li, S. Polymer 2002, 43, 2729.
6. Usuki, A.; Kawasumi, M.; Kojima, Y.; Okada, A.; Karauchi, T.; Kamigaito, O. J Mater Res 1993, 8, 1774.
7. Wei, Y.; Wang, J.; Jia, X.; Yeh, J.-M.; Spellae, P. Polymer 1995, 36, 4535.
8. Macinnes, D.; Funt, B. L. Synth Met 1988, 25, 235.
9. Bergeron, J.-Y.; Chevalier, J. W.; Dao, L. H. J Chem Soc Chem Commun 1990, 180.
10. Sathiyanarayanan, S.; Blakrishnan, K. Electrochim Acta 1994, 39, 831.
11. Biswas, M.; Ray, S. S. J Appl Polym Sci 2000, 77, 2948.
12. Wu, C.-G.; DeGroot, D. C.; Marcy, H. O.; Schindler, J. L.; Kannewurf, C. R.; Liu, Y.-J.; Hirpo, W.; Kanatzidis, M. G. Chem Mater 1996, 8, 1992.
13. Wang, L.; Brazis, P.; Rocci, M.; Kannewurf, C. R.; Kanatzidis, M. G. Chem Mater 1998, 10, 3298.
14. Chao, K.-J.; Ho, S.-Y.; Chang, T.-C. U.S. Pat. 5,340,500, 1994.
15. Giannelis, E.; Mehrota, V. U.S. Pat. 5,032,547 (1991).
16. Choi, H. J.; Kim, J. W.; Kim, S. G.; Kim, B. H.; Joo, J. Polym Mater Sci Eng 2000, 82, 245.

17. Wu, Q.; Xue, Z.; Qi, Z.; Wang, F. Polymer 2000, 41, 2029.
18. (a) Oriakhi, C. O.; Lerner, M. M. Mater Res Bull 1995, 30, 723; (b) Sinharay, S.; Biswas, M. Mater Res Bull 1999, 34, 1187.
19. Akorna, G.; Ugi, I. Angew Chem Int Ed Engl 1977, 16, 259.
20. Nair, C. P. R.; Glouet, G.; Guilbert, Y. Polym Degrad Stab 1989, 26, 305.
21. Yano, K.; Usuki, A.; Okada, A. J Polym Sci Polym Chem Ed 1997, 35, 2289.
22. Wrobleski, D. A.; Benicewicz, B. C.; Thompson, K. G.; Byraan, C. J. Polym Prepr (Am Chem Soc Div Polym Chem) 1994, 35, 265.
23. Gilman, J. W.; Kashiwagi, T.; Lyden, M.; Brown, J. E. T.; Jackson, C. L.; Lomakin, S.; Giannelis, E. P.; Manias, E. Chemistry and Technology of Polymer Additives; Blackwell Scientific: Oxford, 1999; p 249.
24. Gilman, J. W. Appl Clay Sci 1999, 15, 31.
25. Wessling, B. Adv Mater 1994, 6, 226.
26. (a) Khanna, Y. P.; Reimschuessel, A. C.; Banjerie, A.; Altman, C. Polym Eng Sci 1988, 28, 1600; (b) Khanna, Y. P.; Reimschuessel, A. C. J Appl Polym Sci 1988, 35, 2259; (c) Muellerleile, J. T.; Freeman, J. J. J Appl Polym Sci 1994, 54, 135.